RSC Advances

PAPER

View Article Online
View Journal | View Issue

Cite this: *RSC Adv.*, 2022, **12**, 34438

Adsorptive removal of tetracycline and ciprofloxacin drugs from water by using a magnetic rod-like hydroxyapatite and MIL-101(Fe) metal–organic framework nanocomposite†

Maryam Beiranvand,[a] Saeed Farhadi *[a] and Abdolnasar Mohammadi-Gholami[b]

A novel porous nanocomposite composed of hydroxyapatite nanorods (HAP), a MIL-101(Fe) metal–organic framework, and Fe_3O_4 nanoparticles was successfully fabricated in this work. The magnetic HAP/MIL-101(Fe)/Fe_3O_4 ternary nanocomposite was identified by various techniques, namely FT-IR spectroscopy, XRD, Raman spectroscopy, SEM, EDX, TEM, BET specific surface area, zeta potential, and VSM measurements. Tetracycline (TC) and ciprofloxacin (CIP) aqueous solutions were used to evaluate the adsorption performance of the resulting HAP/MIL-101(Fe)/Fe_3O_4 composite. The adsorption rate and capacity of HAP/MIL-101(Fe)/Fe_3O_4 were increased as compared with HAP, MIL-101(Fe), and HAP/MIL-101(Fe) samples due to the increased attraction. The influence of initial drug concentration, adsorbent dosage, temperature, and pH on the adsorption process was investigated. The results showed that the removal efficiencies of HAP/MIL-101(Fe)/Fe_3O_4 for TC and CIP were 95% and 93%, under the determined optimum conditions: pH of 7, drug concentration of 50 mg L^{-1}, adsorbent dosage of 30 mg, and temperature of 25 °C. The maximum adsorption capacities of HAP/MIL-101(Fe)/Fe_3O_4 for TC and CIP were 120.48 mg g^{-1} and 112.35 mg g^{-1}, respectively. Reusability of the prepared nanocomposite was easily achieved up to three times without significant change in its structure. As a result, the synthesized magnetic nanocomposite can be reused as a suitable absorbent for TC and CIP removal from aqueous solutions.

Received 3rd October 2022
Accepted 25th November 2022

DOI: 10.1039/d2ra06213e

rsc.li/rsc-advances

1. Introduction

The removal of pharmaceutical pollutants from polluted water is now a serious environmental problem. Thousands of tons of active pharmaceutical compounds are used to treat diseases, including antibiotics, antipyretics, analgesics, antihypertensives, and so on. Pharmaceutical compounds are discharged into water resources through different pharmaceutical industries, hospitals wastewater and domestic sewages.[1,2] This damages the aquatic ecosystem and besides causing chemical pollution, induces the production of resistant microbes and the resistance genes in the environment, resulting in continuous pollution. Pharmaceutical compounds are increasingly resistant to hydrolysis and biological degradations and their breakdown in the environment is often a slow process. These compounds are moved by the movement of surface and ground waters, and they are transferred from water into the soil and plants, and then to humans and animals.[3] These pollutions can enter the human body through direct or indirect contact with people, and cause great harm to human health.

Among various antibiotics, ciprofloxacin (CIP) and tetracycline (TC) were regarded as a significant threat to the ecosystem and public health due to their high solubility in water, persistence, toxicity, and potential carcinogenicity.[4,5] Therefore, for human health and other living organisms, the treatment of wastewater is imperative. To tackle this problem lots of technologies and methods such as biodegradation,[6] advance oxidation,[7] photo-Fenton process,[8] ozonation,[9] membrane technology,[10] and adsorption[11–13] have been developed. Among the above methods, adsorption technology is a better choice for removing pharmaceutical compounds because of its simplicity, high efficiency, relatively low cost, and no high toxicity by-products. Adsorption is a promising technique for pharmaceutical compounds removal which binds the particles on the surface of the adsorbent by physical or chemical forces. Conventional adsorbents such as activated carbon,[14,15] graphene oxide (GO),[16] zeolite[17] and clays[18] have been used for the removal of pharmaceutical compounds from the wastewater.

Amongst the different adsorbents used, hydroxyapatite (HAP) is an efficient adsorbent. HAP is a unique form of calcium

[a]Department of Chemistry, Lorestan University, Khorramabad, 68151-44316, Iran. E-mail: farhadi.s@lu.ac.ir

[b]Department of Biology, Lorestan University, Khorramabad, 68151-44316, Iran

† Electronic supplementary information (ESI) available. See DOI: https://doi.org/10.1039/d2ra06213e

phosphate having a chemical formula of $Ca_{10}(PO_4)_6(OH)_2$. HAP is well known as the mineral component of bones and teeth. This attractive material possesses excellent biocompatibility, bioactivity, osteoconductivity, bioaffinity and nontoxicity. HAP has been studied for many years, due to its chemical and structural similarity with the mineral constituents of human bones and teeth.[19–23] HAP can accept a large number of anionic and cationic substituents which facilitates the possibility of using it in various applications. HAP is widely used in various applications like nanomedicine, drug and gene delivery, ion conductor, catalyst, biosensor and tissue engineering.

Metal–organic frameworks (MOFs) have evolved as a new class of porous crystalline materials built through coordination bonds between metal ions and organic ligands.[24,25] MOFs have attracted much attention owing to their unique properties, such as biocompatibility, high specific surface area, highly distribution of metallic centers, high pore volume, good thermal, chemical and mechanical stability, easily tunable framework, and versatile functionality. Because of these advantages MOFs, have been applied as potential candidates in various applications, including drug delivery, magnetic resonance imaging, separation materials, gas storage/separation, catalysis, sensors, luminescence, ion exchange, and highly efficient adsorbents.[26–32] Among MOFs, one of the most attractive materials is MIL-101(Fe), (MIL = Materials Institute Lavoisier). MIL-101(Fe) compounds are constructed by iron(III) ions and terephthalic acid, which show fantastic applications in many areas due to their highly porous structure, excellent thermal stability, chemical robustness, environmentally friendly, and low cost. Thus, these features make MIL-101(Fe) to be a suitable candidate for environmental contaminant elimination.

In this paper, a new magnetic ternary nanocomposite, namely HAP/MIL-101(Fe)/Fe_3O_4 was prepared *via* the hydrothermal method. This magnetic nanocomposite was tested for the removal of tetracycline (TC) and ciprofloxacin (CIP) antibiotics from aqueous solutions at different values of pH, temperature, adsorbent dosage, and initial drug concentration. TC and CIP have been selected for this study because they are broad spectrum antibiotics used in treating of a variety of bacterial diseases. To the best of our knowledge, there is no report about the synthesis of HAP/MIL-101(Fe)/Fe_3O_4 nanocomposite and its application in removal of drugs from aqueous solutions. The molecular tructures of TC and CIP drugs are shown in Fig. S1.†

2. Experimental

2.1. Materials and methods

Calcium nitrate tetra hydrate ($Ca(NO_3)_2\cdot4H_2O$, 98%), diammonium hydrogen phosphate ($(NH_4)_2HPO_4$, 98.5%), sodium hydroxide (NaOH, 98%), iron(III) chloride ($FeCl_3\cdot6H_2O$, 99%), terephthalic acid (1,4 BDC, 98%), dimethylformamide (DMF, 99%), ammonium iron(II) sulfate hexahydrate ($(NH_4)_2FeSO_4\cdot6H_2O$, 98%), ammonium iron(III) sulfate ($(NH_4)Fe(SO_4)_2\cdot12H_2O$, 98%), ammonium hydroxide (NH_4OH, 25%), hydrochloric acid (HCl, 37%) were obtained from Merck Chemical Company. Tetracycline ($C_{22}H_{24}N_2O_8$, TC, 99.5%) and ciprofloxacin ($C_{17}H_{18}FN_3O_3$, CIP, 95.5%) drugs were obtained from Exir Pharmaceutics Company (Boroujerd, Iran). All of the chemicals were used without further purification.

2.2. Synthesis of hydroxyapatite (HAP) nanorods

HAP was prepared under hydrothermal conditions. Briefly, $(NH_4)_2HPO_4$ aqueous solution (15 mL, 0.12 M) was added dropwise to the aqueous solution of $Ca(NO_3)_2\cdot4H_2O$ (15 mL, 0.2 M) with a stoichiometric ratio of Ca/P = 1.67. The mixture was stirred for 1 h and the pH was continuously adjusted and maintained at 10 during the reaction with the sodium hydroxide solution. After mixing, the precipitate was dispersed in an ultrasonic bath for 30 min to ensure the homogeneous mixture. The mixture was transferred into a 50 mL Teflon-lined autoclave and heated at 180 °C for 24 h. The precipitate was washed with deionized water several times and finally dried at room temperature for 24 h.

2.3. Synthesis of Fe_3O_4 nanoparticles

In a typical experiment, 0.964 g $(NH_4)Fe(SO_4)_2\cdot12H_2O$ and 0.392 g $(NH_4)_2Fe(SO_4)_2\cdot6H_2O$ were dissolved in 30 mL deionized water. Then, 10 mL NH_4OH was added into the mixed solution, adjusting the pH of the system to 10–11. This mixed solution was stirred vigorously for 1 h at 80 °C. Then, the black color solid product was separated by centrifugation and washed with deionized water and ethanol several times. The final product was dried at 70 °C for 10 h.

2.4. Synthesis of HAP/MIL-101(Fe)

The HAP/MIL-101(Fe) composite was prepared through a hydrothermal procedure. 0.2 g of the as-prepared HAP rods, 0.332 g H_2BDC, and 0.8 g $FeCl_3\cdot6H_2O$ were dispersed into 30 mL DMF by ultrasonic treatment for 15 min. The mixture was stirred for 1 h and then transferred into a 50 mL Teflon-lined autoclave and warmed at 120 °C for 20 h. The obtained precipitate was centrifuged and washed by DMF and ethanol several times. The purified product was dried at 70 °C for 30 min. For a comparison, pure MIL-101(Fe) was also synthesized under the same conditions without the addition of HAP powder.

2.5. Synthesis of magnetic HAP/MIL-101(Fe)/Fe_3O_4 nanocomposite

For the preparation of HAP/MIL-101(Fe)/Fe_3O_4 nanocomposite, 0.5 g of dried HAP/MIL-101 powder was dispersed in 15 mL deionized water. After that, 0.125 g of dried Fe_3O_4 powder was dispersed in 10 mL deionized water with sonicating for 15 min. Then, these two suspensions were mixed. The obtained mixture was stirred for 1 h at ambient temperature. The dark brown solid was washed with deionized water and dried at 70 °C for 1 h. The weight percentage values of HPA, MIL101(Fe) and Fe_3O_4 components in the nanocomposite based on consumed starting materials were calculated to be 50%, 30% and 20%, respectively. Then, HAP is the main component of composite.

2.6. Characterization methods

The FT-IR spectrum was registered by a Shimadzu-8400S (Japan) spectrometer in the wavenumber range of 400–4000 cm^{-1} using KBr pellets. Powder X-ray diffraction (PXRD) patterns were analyzed by a Rigaku D/Max C III diffractometer using nickel-filtered Cu Kα radiation ($\lambda = 40$ 1.5406). Raman spectra of the samples were recorded using a Raman microscope (Model: SENTERRA 2009, Germany) with a laser 785 nm. The UV-visible absorption spectra of samples were obtained on a (Cary 100, VARIAN) spectrophotometer. The morphology and elemental analysis of samples were observed using a scanning electron microscopy system (SEM, MIRA3 TESCAN) coupled with energy-dispersive X-ray analysis (EDX). Transmission electron microscopy (TEM) analysis was conducted on a Philips CM120 microscope at the accelerating voltage of 200 kV. BET measurements were performed by N_2 adsorption isotherm with the BET method (Micro metrics PHS-1020, made in Japan). VSM measurements were determined using a vibrating magnetometer MDKFD (Daneshpajooh Co., Kashan, Iran) with a high magnetic field of 10 kOe. Zeta potential measurements were obtained by using a Malvern zeta meter system (Malvern, UK) equipped with a standard 628 nm laser.

2.7. Adsorption tests

Firstly, the aqueous supply solutions (200 mg L^{-1}) of antibiotics were fabricated by dissolving TC and CIP powders in distilled water. Then, the solutions of CIP and TC were achieved with consecutive dilutions using distilled water. The concentrations of TC and CIP were determined using the UV-vis spectrophotometer at 375 and 325 nm, respectively. To obtain the favorable adsorption conditions, the following parameters were studied: initial antibiotic concentration (25–100 mg L^{-1}), adsorbent dosage (15, 30, and 45 mg), pH of the solution (2–10), and the effect of temperature (25, 40, 55, and 70 °C). For investigating the effect of the initial antibiotic concentration, 30 mg of the magnetic adsorbent was added in 50 mL of TC and CIP aqueous solution *via* a concentration between 25–100 mg L^{-1}. The pH of the TC and CIP solutions was adjusted *e* TC and CIP solutions was adjusted in the range of 2–10 by adding HCl or NaOH aqueous solutions. According to the following eqn (1), the equilibrium adsorption capacity q_e (mg g^{-1}) could be computed:

$$q_e = (C_0 - C_t) \times V/m \quad (1)$$

The elimination efficiency, R (%), of the antibiotic by the nanocomposite was computed using eqn (2):

$$R\,(\%) = (C_0 - C_t) \times 100/C_0 \quad (2)$$

where, C_0 and C_t (mg L^{-1}) represent the antibiotic concentration at initial and t times, respectively. V (L) is the volume of the solution and m (g) is the mass of the adsorbent.

3. Results and discussion

The preparation process of HAP/MIL-101(Fe)/Fe_3O_4 nanocomposite was summarized in Scheme 1. The structure and morphology of the nanocomposite were characterized by the means of FT-IR, XRD, Raman, SEM, EDX, TEM, zeta potential, VSM and BET analyses.

3.1. FTIR analysis

The FT-IR spectra of (a) HAP, (b) MIL-101(Fe), (c) Fe_3O_4, (d) HAP/MIL-101(Fe) and (e) HAP/MIL-101(Fe)/Fe_3O_4 are displayed in Fig. 1. In Fig. 1(a), the adsorption bands observed at 1035, 1093 and 567, 603 cm^{-1} corresponds to the asymmetric stretching vibration (ν_3) and bending vibration (ν_4) of phosphate groups. The symmetrical stretching vibration (ν_1 and ν_2) of phosphate groups were observed at 960 and 466 cm^{-1}. The stretching vibrational modes of the OH^- ions were detected at around 3550 and 631 cm^{-1}, respectively.[19,33] The FTIR spectrum of MIL-101(Fe) (Fig. 1(b)), the two strong peaks at 1598 and 1390 cm^{-1} are assigned to the asymmetric and symmetric stretching of carboxyl groups (O–C–O) in BDC, respectively. Also, the peak at 750 cm^{-1} is assigned to the out-of-plane bending vibration of

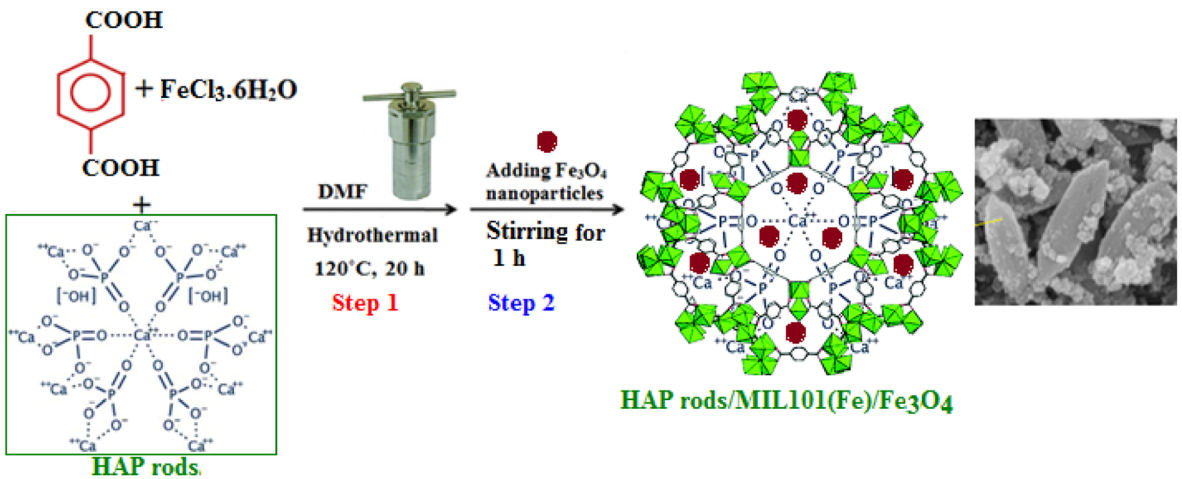

Scheme 1 A schematic representation of the synthesis procedure of HAP/MIL-101(Fe)/Fe_3O_4 nanocomposite.

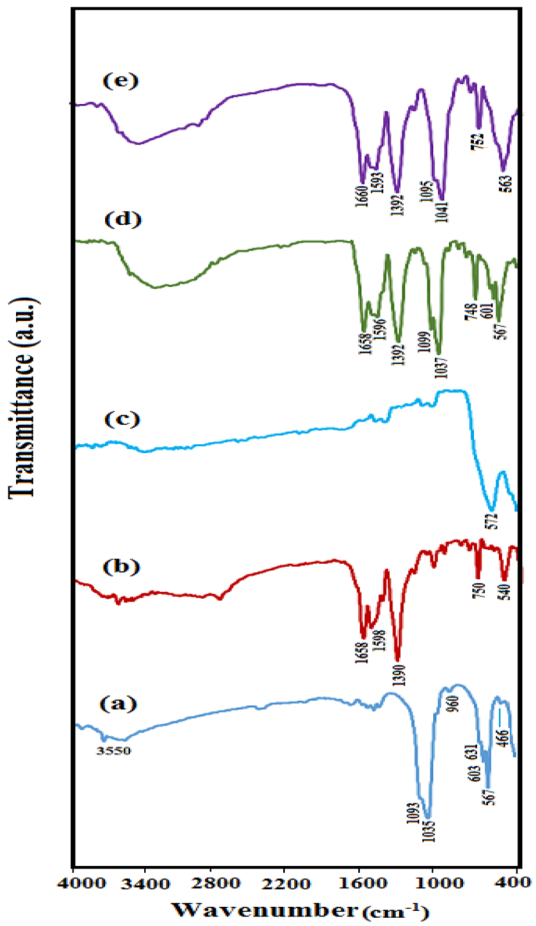

Fig. 1 FT-IR spectra of (a) pure HAP, (b) MIL-101(Fe), (c) Fe_3O_4, (d) HAP/MIL-101(Fe) and (e) HAP/MIL-101(Fe)/Fe_3O_4 nanocomposite.

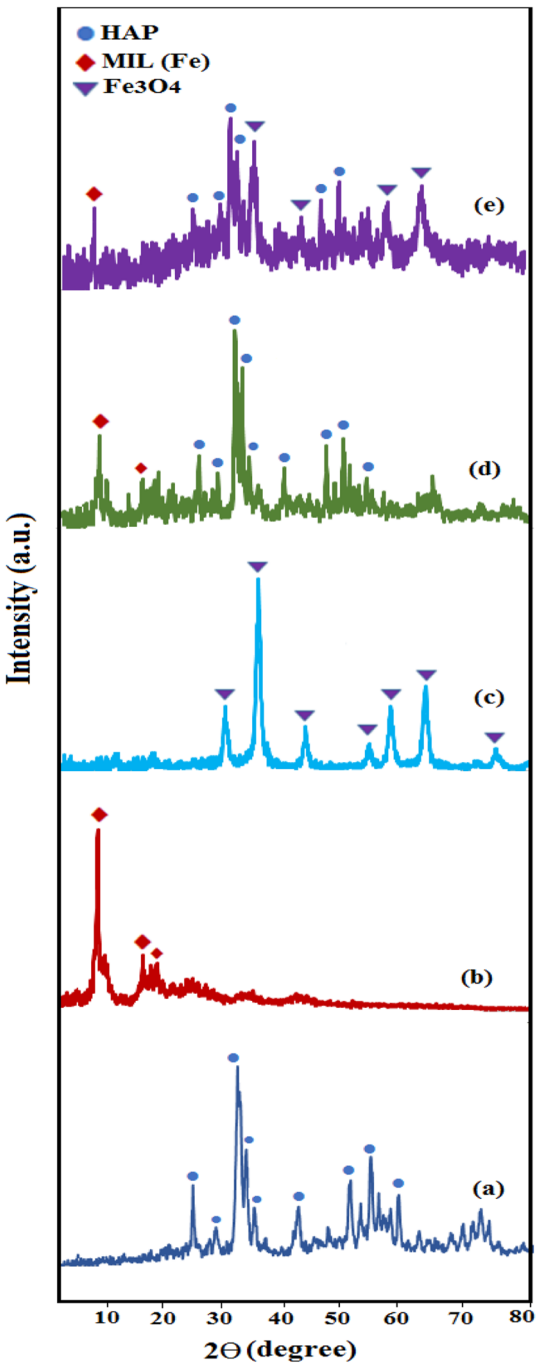

Fig. 2 XRD patterns of (a) pure HAP, (b) MIL-101(Fe), (c) Fe_3O_4, (d) HAP/MIL-101(Fe) and (e) HAP/MIL-101(Fe)/Fe_3O_4 nanocomposite.

C–H groups in the benzene ring of BDC. Moreover, the apparent peak at 540 cm^{-1} is attributed to the Fe–O vibration.[34] As revealed in Fig. 1(c), the intrinsic peak at 572 cm^{-1} is attributed to the vibrational band of the Fe–O of Fe_3O_4.[34] For HAP/MIL-101(Fe) and HAP/MIL-101(Fe)/Fe_3O_4 nanocomposites (Fig. 1(d) and (e)), co-existence of characteristic peaks, confirms attendance of MIL-101(Fe) and Fe_3O_4 on the surface HAP. In Fig. 1(e), the Fe_3O_4 peak could not be observed since the characteristic Fe–O band at 572 cm^{-1} overlapped with the phosphate peaks of HAP at 567 and 603 cm^{-1}.

3.2. XRD analysis

The phase purity and crystal structure of the synthesized samples (a) HAP, (b) MIL-101(Fe), (c) Fe_3O_4, (d) HAP/MIL-101(Fe) and (e) HAP/MIL-101(Fe)/Fe_3O_4 were analyzed by XRD. As exhibited in Fig. 2(a), the major diffraction peaks appeared at 2θ around 25.9°, 32°, 33°, 34.1°, 39.8°, 46.7°, and 50° corresponds to the (002), (211), (300), (202), (310), (222), and (321) reflections of rod-like structure of hydroxyapatite (JCPDS card no. 09-0432).[19,35] The XRD pattern of MIL-101(Fe) in Fig. 2(b), showed peaks at $2\theta = 9.66°$, 16.7° and 18.88° which assigned to the (119), (115), and (224) planes, respectively.[34] From Fig. 2(c), the characteristic diffraction peaks of Fe_3O_4 particles are observed at $2\theta = 30.2°$, 35.6°, 43.3°, 53.7°, 57.3°, and 62.8° assigning to (220), (311), (400), (422), (511), and (440) the crystal planes (JCPDS card no. 19-0629).[34,36] In Fig. 2(d) and (e), the XRD patterns for the HAP/MIL-101(Fe) and HAP/MIL-101(Fe)/Fe_3O_4 nanocomposites indicated the phase of HAP, Fe_3O_4, and MIL-101(Fe). These findings clearly confirm the formation of nanocomposite without any impurity phases.

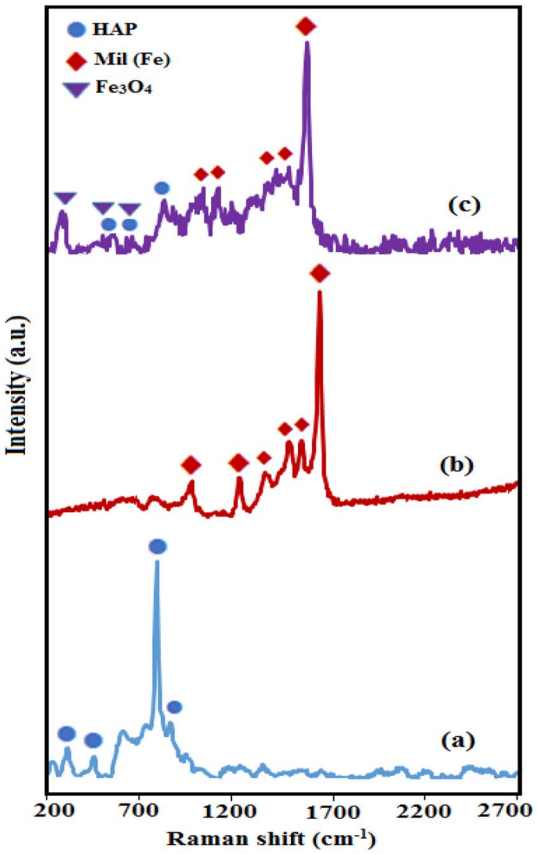

Fig. 3 Raman spectra of (a) pure HAP, (b) MIL-101(Fe) and (c) HAP/MIL-101(Fe)/Fe_3O_4 nanocomposite.

3.3. Raman analysis

The Raman spectroscopy was used to complete the structural analysis of HAP, MIL-101(Fe), HAP/MIL-101(Fe)/Fe_3O_4 nanocomposite. As shown in Fig. 3(a), the Raman peaks of the HAP phase were appeared at 470, 572, 960 and 1035 cm^{-1}. These peaks were related to the ν_2 (PO_4^{3-}), ν_4 (PO_4^{3-}), ν_1 (PO_4^{3-}), ν_3 (PO_4^{3-}) vibration modes of the phosphate groups, respectively.[19] Based on Fig. 3(b), the vibrational bands of MIL-101(Fe) were observed at 862, 1138, 1292, 1431, 1504, and 1613 cm^{-1} indicating aromatic and dicarboxylate groups in BDC.[24] The Raman spectrum of the magnetic nanocomposite in Fig. 3(c) showed three bands of Fe_3O_4 at 200, 680, and 757 cm^{-1} and several peaks of the MIL-101(Fe), besides the characteristic bands of HAP with lower intensities, which may be due to chemical interaction between HAP and MIL-101(Fe). Raman spectra again confirmed the successful synthesis of HAP/MIL-101(Fe)/Fe_3O_4 composite.

3.4. SEM and EDX analysis

Fig. 4 shows the SEM images of the as-prepared pure HAP and HAP/MIL-101(Fe)/Fe_3O_4 nanocomposite in various magnifications. Based on Fig. 4(a), pure HAP particles have a regular rod like morphology with a diameter size of about 40 nm and a length up to 150 nm. Fig. 4(b)–(d), confirmed the successful growth of Fe_3O_4 particles and MIL-101(Fe) on the HAP nanorods. After the addition of MIL-101(Fe) and Fe_3O_4 the diameter size of the HAP particles increased, but its morphology remained unchanged. Also, these images, especially image 4(d) with higher resolution, shows that the MIL-101(Fe) and Fe_3O_4 particles have been homogeneously dispersed on the HAP rods.

3.5. TEM analysis

To further confirm the structure and morphology of HAP/MIL-101(Fe)/Fe_3O_4 composite, the TEM of the sample was also investigated. The TEM images of HAP/MIL-101(Fe)/Fe_3O_4 nanocomposite are shown in Fig. 5. The sample was dispersed in ethanol under the ultrasonic vibration for TEM measurements. The TEM images in Fig. 5, show that the nanocomposite was formed mainly from rod-like particles. These images showed that the HAP/MIL-101(Fe)/Fe_3O_4 nanocomposite contains a rod-like structure with the lengths of 300–800 nm and diameter sizes of 180–200 nm. From the images, it can be clearly seen that the MIL-101(Fe) and Fe_3O_4 particles were well distributed on the HAP rods. Moreover, the morphology of the HAP/MIL-101(Fe)/Fe_3O_4 composite from TEM images agreed with the SEM results.

3.6. EDX analysis

EDX analysis was used to confirm the composition of the as-prepared nanocomposite. The EDX analysis in Fig. 6(a) indicated Ca, P, C, O and Fe peaks which, confirmed the presence of HAP, MIL-101(Fe) and Fe_3O_4 and is consistent with the results obtained from XRD patterns. Moreover, the EDX elemental mapping in Fig. 6(b), provides the clearer information about distribution of Ca, P, C, O, Fe elements in the nanocomposite which, confirms the homogeneity of the sample.

3.7. Magnetic properties

For the further investigation of the magnetic property of the samples, the magnetic hysteresis loops of Fe_3O_4 nanoparticles and HAP/MIL-101(Fe)/Fe_3O_4 nanocomposite are studied using a vibrating sample magnetometer with the applied magnetic field ranging from −10 000 to 10 000 G at room temperature. From Fig. 7, saturation magnetizations (M_s) values of the pure Fe_3O_4 and HAP/MIL-101(Fe)/Fe_3O_4 nanocomposite can be estimated to be 72, and 10 emu g^{-1}, respectively. The M_s of the magnetic HAP/MIL-101(Fe)/Fe_3O_4 composite decreased compared with that of pure Fe_3O_4, which may be attributed to the reduction of the magnetic source component (Fe_3O_4) per gram in the HAP/MIL-101(Fe)/Fe_3O_4 nanocomposite. However, the magnetization of synthesized HAP/MIL-101(Fe)/Fe_3O_4 composite is strong enough that it can be easily attracted by an external magnetic field. This property is not seen in pure HAP, MIL-101(Fe) and or HAP/MIL-101(Fe).

3.8. BET specific surface areas analysis

The surface area and pore size distribution of pure HAP, MIL-101(Fe) and HAP/MIL-101(Fe)/Fe_3O_4 nanocomposite are studied by N_2 adsorption/desorption measurements. Fig. 8(a–c) shows the BET surface area and their corresponding BJH plot

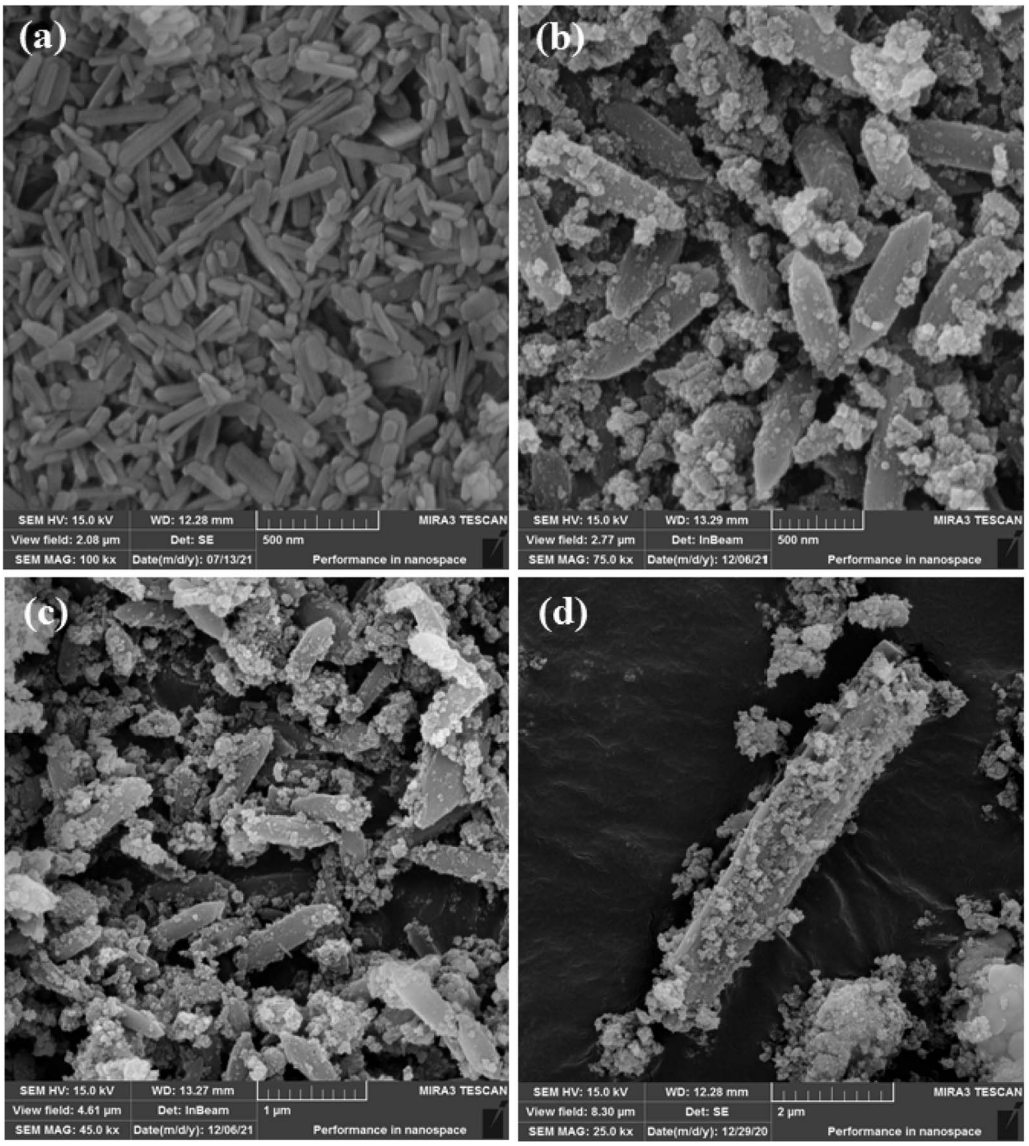

Fig. 4 (a) SEM image of pure HAP and (b)–(d) SEM images of the HAP/MIL-101(Fe)/Fe_3O_4 nanocomposite.

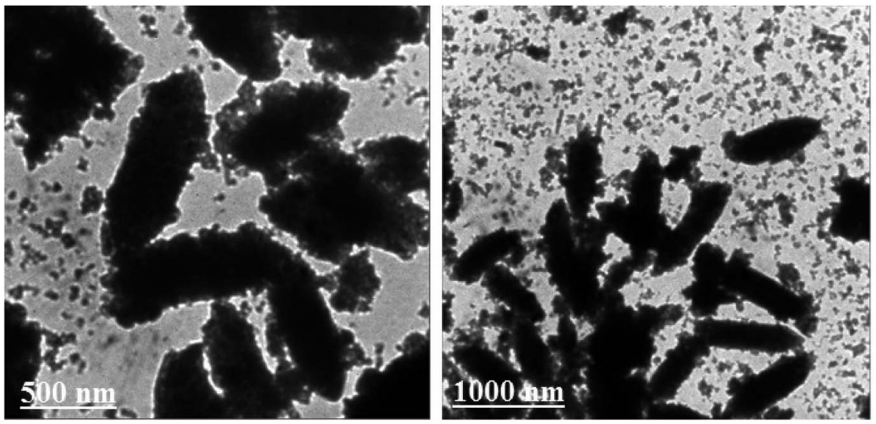

Fig. 5 TEM images of the HAP/MIL-101(Fe)/Fe_3O_4 nanocomposite.

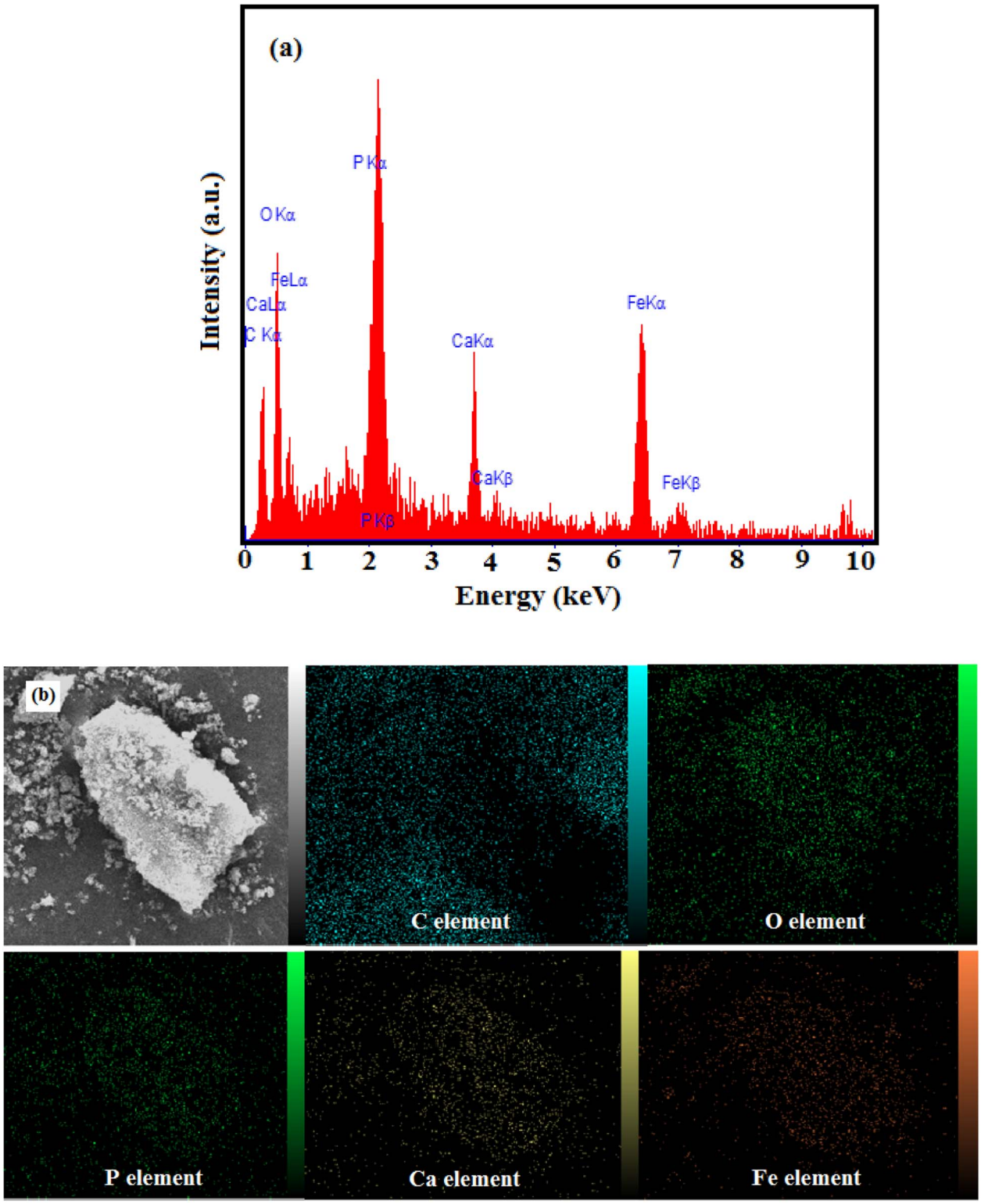

Fig. 6 (a) EDX spectrum and (b) elemental mappings of the HAP/MIL-101(Fe)/Fe_3O_4 nanocomposite.

for pore size distribution. The isotherm curves of HAP and MIL-101(Fe) exhibited type IV plots, according to the IUPAC classification, confirming their mesoporous structures. The pore size distribution of HAP/MIL-101(Fe)/Fe_3O_4 composite shows three peak with pores size in the range of 2–100 nm, indicating the existence of meso- and microporous structures in the nanocomposite. The wide pores size of nanocomposite is beneficial for the adsorption of drugs with different molecular sizes. The calculated BET results showed that the addition of MIL-101(Fe) and Fe_3O_4 particles decreased the surface area of the HAP/MIL-

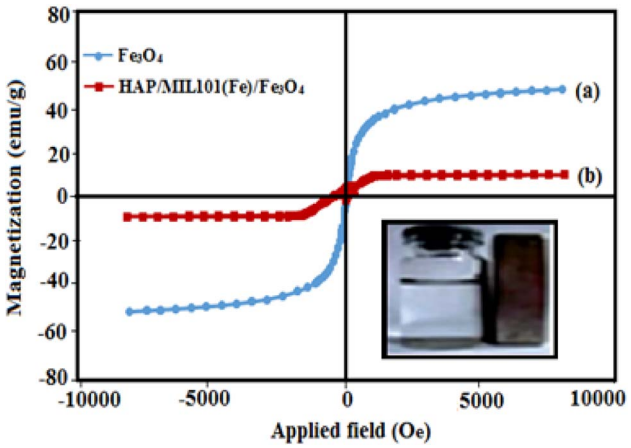

Fig. 7 Magnetization curves of (a) pure Fe_3O_4 and (b) HAP/MIL-101(Fe)/Fe_3O_4 nanocomposite at room temperature (inset: the magnetic separation of HAP/MIL-101(Fe)/Fe_3O_4 nanocomposites by a magnet).

101(Fe)/Fe_3O_4 composite (14 m^2 g^{-1}) compared with pure HAP (224 m^2 g^{-1}), which may be due to blockage of the pores. Some textural properties of the samples were listed in Table 1.

3.9. Zeta potential measurements

The zeta potential of a material is a key factor influencing its adsorption ability. In order to study the surface charge properties of the as-obtained samples, zeta potential measurements were performed in water at natural pH (pH ≈ 6.5–7) and results are shown in Fig. 9. The zeta potential of pure HAP and pure MIL-101(Fe) were measured to be −7.8 and +32.4 mV, respectively (Fig. 9(a) and (b)) while the zeta potential of HAP/MIL-101(Fe)/Fe_3O_4 composite was measured to be +13.6 mV (Fig. 9(c)) while the surface charges of the composite become more positive of +13.6 mV. This significant change in zeta potential value (from −7.8 to +13.6) is most due to the introduction of highly positive charged MIL-101(Fe) component into the structure of HAP as the main component of composite. The

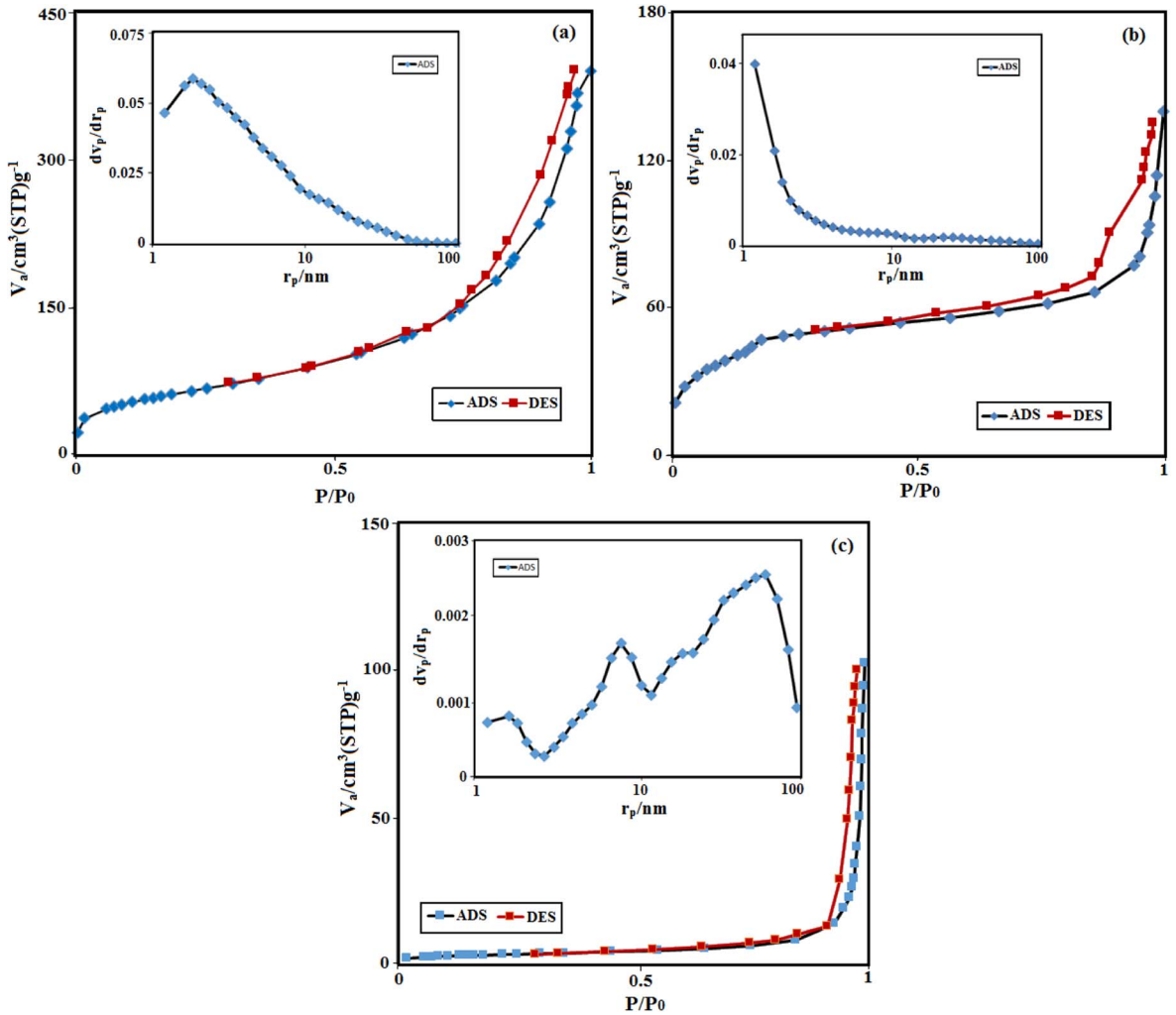

Fig. 8 Nitrogen adsorption–desorption isotherms of (a) pure HAP, (b) MIL-101(Fe) and (c) HAP/MIL-101(Fe)/Fe_3O_4 nanocomposite. The insets show the corresponding pore size distribution curves.

Table 1 Textural properties of the samples

Sample	S_{BET} ($m^2\ g^{-1}$)	S_{Lan} ($m^2\ g^{-1}$)	V_{total} ($cm^3\ g^{-1}$)	D_p (nm)
HAP	224	173	0.59	10.6
MIL-101(Fe)	167	134	0.2	4.7
HAP/MIL-101(Fe)/Fe_3O_4	14	17	0.16	45.8

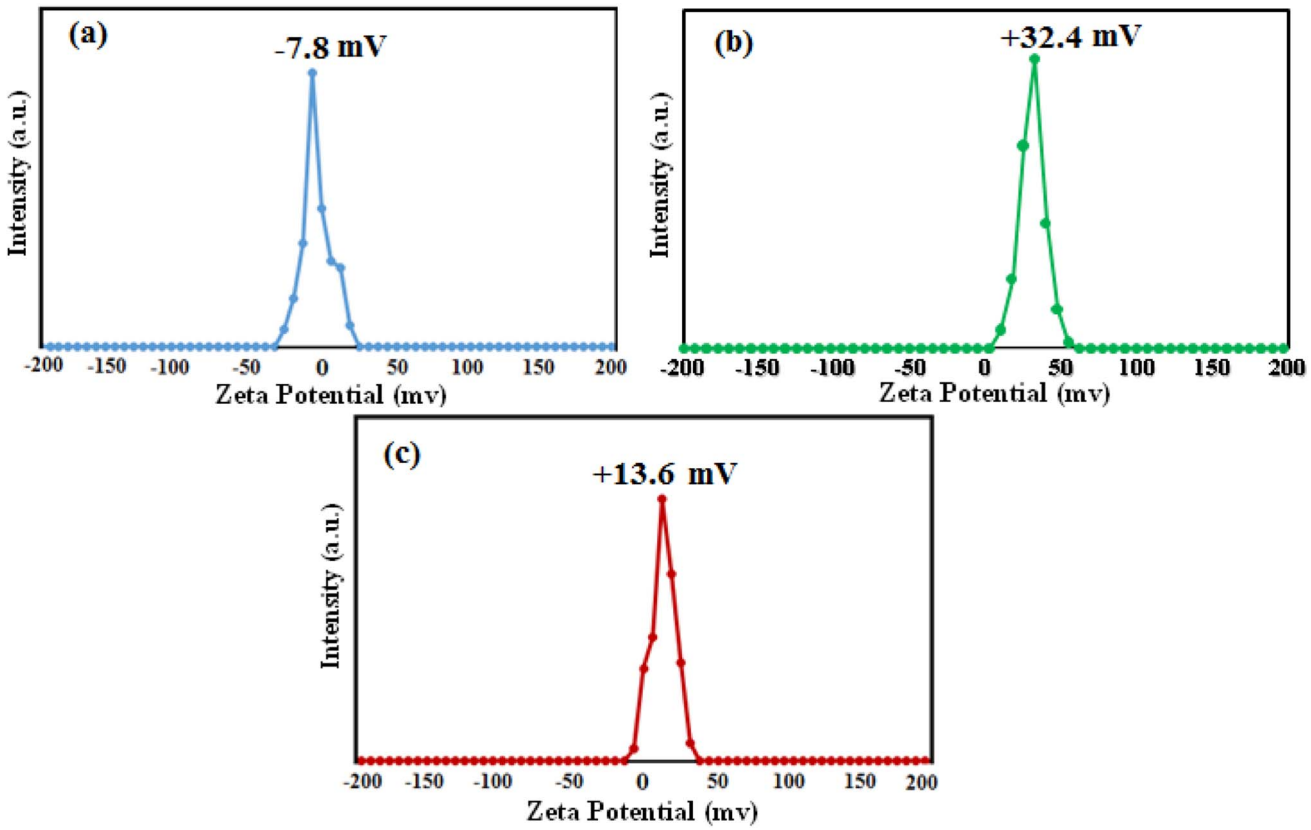

Fig. 9 Zeta potential curves of (a) pure HAP, (b) MIL-101(Fe) and (c) HAP/MIL-101(Fe)/Fe_3O_4 nanocomposite in water at natural pH.

results indicate that the surface of the HAP/MIL-101(Fe)/Fe_3O_4 had a more positive charge under neutral pH compared with that of the initial HAP. That is, the introduction of MIL-101(Fe) MOF can endow HPA for anionic species adsorption, because the adsorbent should be negatively charged in the solutions with neutral or basic pH values higher than the pH point of zero charge (pH_{pzc}). As can be seen in Fig. 9, compared to the zeta potential of pure HAp, the zeta potential of adsorbent increases remarkably with the introduce of MIL101(Fe), which is in favor of the adsorption of anionic species.

3.10. Antibiotics adsorption studies

To evaluate the efficiency of HAP/MIL-101(Fe)/Fe_3O_4 nanocomposite in the elimination of antibiotics from contaminated water, two model antibiotics (TC, CIP) for the experiments were selected. UV-vis spectra of antibiotics adsorption by the HAP/MIL-101(Fe)/Fe_3O_4 are presented in Fig. 10. As shown in Fig. 10, the intensity of the peaks diminished with the adsorption time due to the decrease of antibiotic concentration in the solution. The removal efficiency for TC is 95% in 20 min as well as for CIP is 93% in 25 min.

3.10.1. Effect of solution pH. The solution pH is the main parameter in the adsorption method, which can influence the charges of the adsorbent and the adsorbate as well as the adsorption mechanism. In order to examine the influence of pH in the elimination of TC and CIP by HAP/MIL-101(Fe)/Fe_3O_4 nanocomposite, the solution was investigated in the pH range of 2–10, while other parameters such as the adsorbent dosage, and initial antibiotic concentration were fixed with the values of 30 mg and 50 mg L^{-1} at 25 °C. The influence of solution pH on the removal of TC antibiotic has been shown in Fig. 11(a). It can be clearly observed that the adsorption capacity increased when the pH of the solution increased gradually from 2 to 10. The maximum removal percentage is reached at pH 10. This behavior is due to the proprieties of HAP/MIL-101(Fe)/Fe_3O_4 nanocomposite and the nature of the TC molecule. As reported in literature, TC molecule has four pK_a of 3.3, 7.7, 9.7 and 12

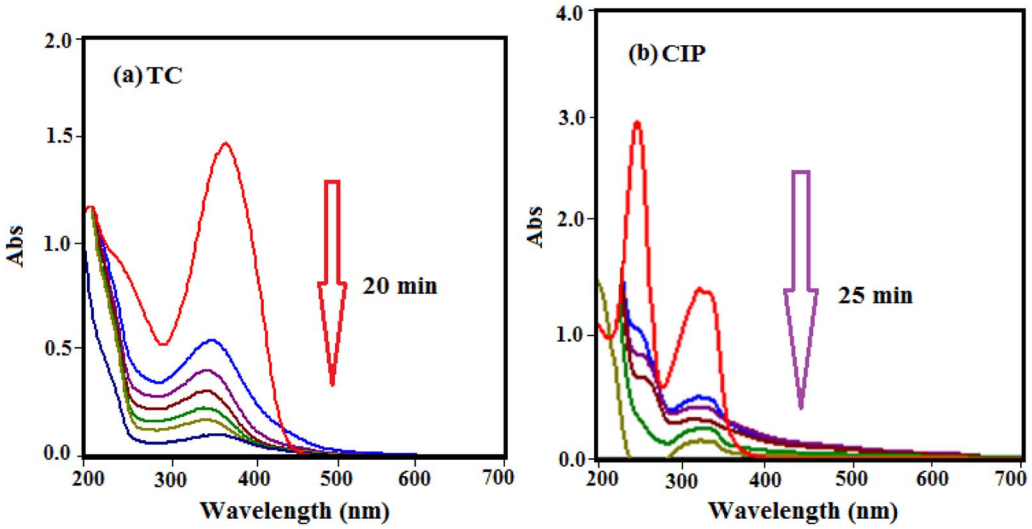

Fig. 10 UV-vis spectral changes of drugs aqueous solutions with HAP/MIL-101(Fe)/Fe_3O_4 at different time intervals: (a) TC and (b) CIP (experimental conditions: $[drug]_0 = 50$ mg L^{-1}, $V = 50$ mL, adsorbent dose: 30 mg at 25 °C).

with ionic species of TC^+ at pH < 3.3, $TC^{\pm}$ at 3.3 < pH < 7.7, TC^- at 7.7 < pH < 9.7 and TC^{2-} at pH > 9.7 (see Fig. S2†).[37] When the pH value is less than 8, the electrostatic repulsion between the adsorbent and adsorbate decreases adsorption capacity, while the pH value is greater than 8, the electrostatic attraction increases the adsorption capacity. Also, the CIP molecule has two pK_as at 6.1 and 8.7. CIP species are cationic CIP^+ at pH < 6.1, zwitterionic $CIP^{\pm}$ at 6.1 < pH < 8.7, and anionic CIP^-/CIP^{2-} at pH > 8.7 (see Fig. S3†).[37] As shown in Fig. 11(a), the adsorption capacity of HAP/MIL-101(Fe)/Fe_3O_4 for CIP increased with the solution pH increasing from 2.0 to 7.0. On the other hand, the adsorption capacity decreased with the increasing pH from 7 to 10. The maximum removal percentage is reached at about pH 7, which corresponds to the zwitterions ($CIP^{\pm}$) zone of the CIP. When the CIP is in zwitterical or neutral form, its solubility decreases, which increases the adsorption capacity.[38]

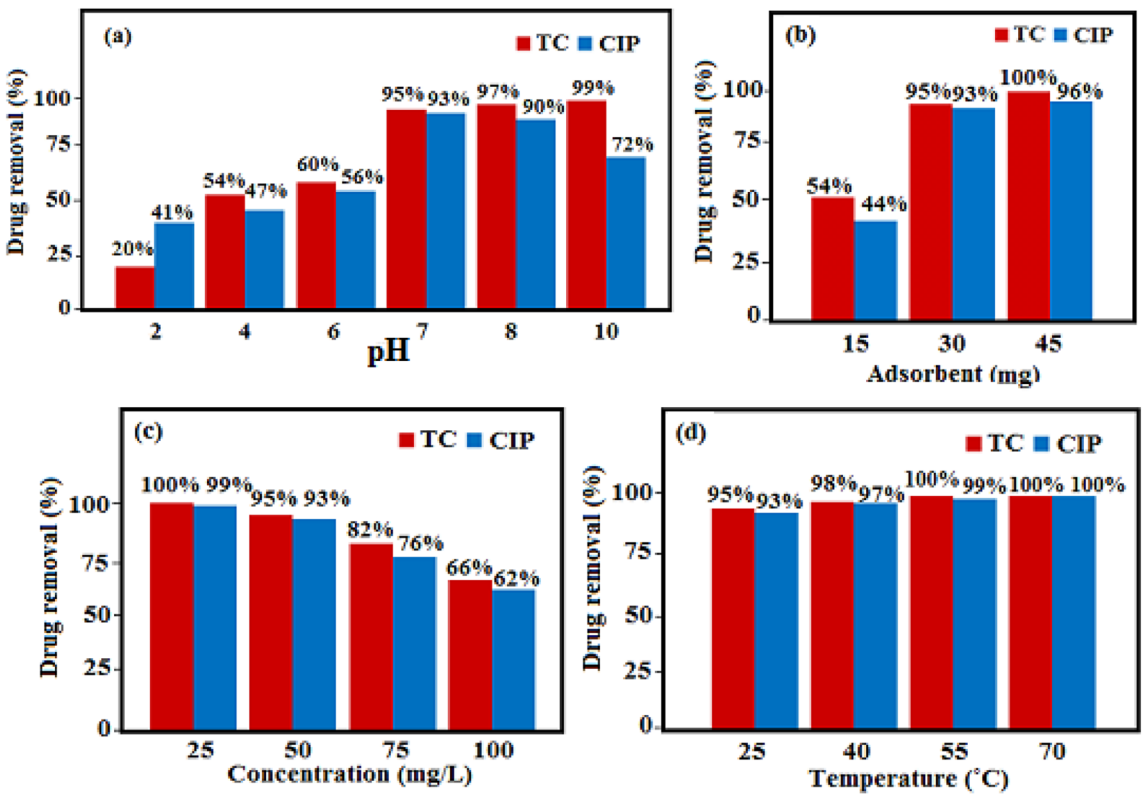

Fig. 11 Effects of (a) pH, (b) antibiotic concentration, (c) adsorbent dosage and (d) temperature on the removal of TC and CIP antibiotics.

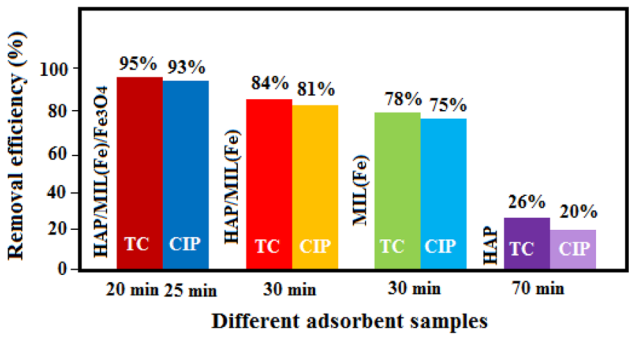

Fig. 12 Removal efficiency of the nanocomposite components.

3.10.2. Effect of adsorbent dose. The influence of the adsorbent dosage was studied in the range of 15–45 mg with 50 mg L^{-1} initial concentration, pH 7, and 25 °C. Fig. 11(b) displayed the percentage of removal of antibiotic increases with the increase of the adsorbent dose, due to the presence of more active sites.[34,37] As shown in Fig. 11(b), the adsorption reached its maximum with 45 mg of adsorbent, and the maximum removal efficiency for TC and CIP was 100 and 96%, respectively.

3.10.3. Effect of the initial concentration of antibiotic. Another parameter that influences on the antibiotic removal rate using HAP/MIL-101(Fe)/Fe_3O_4 nanocomposite, is the initial concentration of antibiotic. The effect of the various initial concentrations (25, 50, 75, and 100 mg L^{-1}) of TC and CIP on the adsorption onto the HAP/MIL-101(Fe)/Fe_3O_4 nanocomposite under the constant conditions of 30 mg absorbent, pH 7, and 25 °C were presented in Fig. 11(c). It was found enhancing the initial antibiotic concentration, the removal of antibiotic decreases. This may occur due to saturation of accessible active sites on the surface of the adsorbent.[34,39]

3.10.4. Effect of temperature. The influence of reaction temperature on the elimination of antibiotics from aqueous solutions *via* HAP/MIL-101(Fe)/Fe_3O_4 was investigated at four temperatures (25, 40, 55, and 70 °C) under the constant conditions of 50 mg L^{-1} initial concentration, 30 mg adsorbent, and pH 7. As shown in Fig. 11(d). The highest percentage of elimination is reached at 70 °C. Increasing the adsorption capacity with enhancing temperature shows that the adsorption is an endothermic process ($\Delta H^\circ > 0$). The increase of temperature leading to an enhancing rate of the antibiotic diffusion in the depth of the adsorbent and occupying all the available vacant sites.[24,34] In addition, the adsorption of drugs onto the HAP/MIL-101(Fe)/Fe_3O_4 composite is accompanied with high randomness and increased defects at the solid/solution interface ($\Delta S^\circ > 0$). The positive enthalpy change ($\Delta H^\circ > 0$) and positive entropy change ($\Delta S^\circ > 0$) resulted in negative Gibbs free energy change ($\Delta G^\circ = (\Delta H^\circ - T\Delta S^\circ) < 0$), indicating that the adsorption process of drugs is spontaneous and favorable at different temperatures.

3.10.5. Removal efficiency of the nanocomposite components. The removal efficiency of pure HAP, MIL-101(Fe), and HAP/MIL-101(Fe) in the elimination of TC and CIP from aqueous solutions were studied under the optimum reaction conditions (Fig. 12). The removal efficiency of these components to TC as well as CIP was 26–95% and 20–93% after adsorption times of 20–70 minutes and 25–70 minutes, respectively. The elimination percentage of the HAP/MIL-101(Fe)/Fe_3O_4 nanocomposite is higher than the individual components and HAP/MIL-101(Fe) composite, which indicated magnetic nanocomposite is a better choice for the antibiotics removal. Due to the presence of magnetic Fe_3O_4, it can be recoverable easily from the mixture by a magnet.

Table 2 Comparison of the adsorption capacities of some typical adsorbents for TC and CIP adsorption

Adsorbent	Drug	Reaction conditions	q_m (mg g^{-1})	Ref.
MGO	TC	Adsorbent 66.6 mg, TC 50 mg L^{-1}, pH 4–5, 40 °C	106.60	40
GO/g-C_3N_4-Fe_3O_4	TC	Adsorbent 30 mg, TC 50 mg L^{-1}, pH 3, 25 °C	107.28	41
Fe_3O_4-g-CN@PEI-b-CD	TC	Adsorbent 800 mg, TC 265 mg L^{-1}, pH 9.2, 47 °C	833.33	42
MWCNT/MIL-53(Fe)	TC	Adsorbent 200 mg, TC 20 mg L^{-1}, pH 7, 25 °C	180.68	43
HAP/ZnO-1	TC	Adsorbent 150 mg, TC 50 mg L^{-1}, pH 5, 25 °C	33.97	44
HAP/ZnO-2	TC	Adsorbent 100 mg, TC 50 mg L^{-1}, pH 5, 25 °C	100.55	44
HAP/ZnO-3	TC	Adsorbent 100 mg, TC 50 mg L^{-1}, pH 5, 25 °C	168.46	44
CoO@C	TC	Adsorbent 100 mg, TC 50 mg L^{-1}, pH 8, 450 °C	769.43	45
CDF@MF	TC	Adsorbent 10 mg, TC 100 mg L^{-1}, pH 6, 25 °C	168.24	46
Co-SCG	TC	Adsorbent 100 mg, TC 0.2 mM, pH 7, 25 °C	370.37	47
Z-HAP-AA	TC	Adsorbent 100 mg, TC 100 mg L^{-1}, pH 3.3, 30 °C	186.09	48
$MnFe_2O_4$/rGO	TC	Adsorbent 5 mg, TC 10 mg L^{-1}, pH 3.3, 25 °C	41	49
PPJ	CIP	Adsorbent 1 mg, CIP 100 mg L^{-1}, pH 4, 25 °C	250	50
MIL101(Cr)-HSO_3	CIP	Adsorbent 100 mg, CIP 120 mg L^{-1}, pH 8, 30 °C	564.9	51
Fe_3O_4/cellulose	CIP	Adsorbent 20 mg, CIP 15 mg L^{-1}, pH 7, 25 °C	168.03	52
Fe/Zn-SBC	CIP	Adsorbent 500 mg, CIP 20 mg L^{-1}, pH 6, 25 °C	74.2	37
CPS	CIP	Adsorbent 100 mg, CIP 60 mg L^{-1}, pH 5, 25 °C	92.45	53
MGO@PANI	CIP	Adsorbent 20 mg, CIP 50 mg L^{-1}, pH 6, 25 °C	106.38	54
Fe_3O_4-MoO_3-AC	CIP	Adsorbent 10 mg, CIP 20 mg L^{-1}, pH 6–8, 25 °C	44.64	55
HAP/MIL101(Fe)/Fe_3O_4	CIP	Adsorbent 30 mg, CIP 50 mg L^{-1}, pH 7, 25 °C	112.35	This work
HAP/MIL101(Fe)/Fe_3O_4	TC	Adsorbent 30 mg, TC 50 mg L^{-1}, pH 7, 25 °C	120.48	This work

3.10.6. Comparison of the adsorption capacities of some typical adsorbents for TC and CIP adsorption. In order to show the advantage of the present adsorbent, we have compared the obtained results in the removal of TC and CIP from aqueous solution by HAP/MIL-101(Fe)/Fe_3O_4 nanocomposite with some reported similar adsorbents in the literature.[37,40–55] From Table 2, it is clear that with respect to the reaction conditions and the adsorption capacities, the present method is more suitable and/or superior. The adsorption process in the presence of some reported adsorbents showed lower adsorption capacities compared to the HAP/MIL-101(Fe)/Fe_3O_4 nanocomposite. However, as can be seen in the table the adsorbents such as Fe_3O_4-g-CN@PEI-b-CD and CoO@C have higher capacities than our adsorbent but higher adsorbent dose used and the preparation process and/or recovery these adsorbent are difficult. The MIL-101(Fe) MOF with a large positive charges incorporated in the hybrid has a stronger attraction force with the negative charges of anionic species of drugs. In fact, the higher adsorption capacity of the HAP/MIL-101(Fe)/Fe_3O_4 nanocomposte is due to the synergistic effect between MIL-101(Fe) and HPA.

3.11. Possible adsorption mechanism

The adsorption mechanism of a TC and CIP on the surface of an adsorbent is depending on numerous factors, including the adsorbent properties, the drug nature, electrostatic interaction, π–π interaction, hydrogen bonding, van der Waals forces and surface complexation.[56] From the adsorption data of TC, it was found that the maximum adsorption occurs at pH = 10 and TC by the electrostatic interaction between the positive charge surface of the adsorbent (mainly due to the presence of MIL-101 as confirmed by zeta potential data in Fig. 9) and the negative charge TC species (TC^- and TC^{2-} anions). On the other hand, for CIP the maximum adsorption occurs at pH = 7 which corresponds to the zwitterions ($CIP^{\pm}$) zone of the CIP. Also in this work, the adsorption efficiency of HAP/MIL-101(Fe)/Fe_3O_4 was found to be higher as compared to pure HAP, MIL-101(Fe), and HAP/MIL-101(Fe). This result indicates that there are other factors influencing the adsorption efficiency besides the electrostatic interaction. The simplified mechanism of TC and CIP drugs adsorption is illustrated in Fig. 13. First, there are many open metal sites on MIL-101(Fe) MOF that facilitate the adsorption of guest drug molecules with corresponding functional groups.[57–59] Secondly, the large specific surface area and large pores of the MIL-101(Fe) MOF benefit the diffusion of drug molecules from the solution to the outer surface of HAP/MIL-101(Fe)/Fe_3O_4 as well as the pores and inner surface.[60] In addition, the aromatic structure of the drugs molecule can interact with the benzene ring of the composite organic moiety through a π–π interaction.[61] The O-containing groups in MIL-101(Fe) and HAP play an important role in the adsorption process. At the same time, hydrogen bonding may occur between functional groups of drugs such as OH, NH_2 and carbonyl groups and O-containing groups of the HAP/MIL-101(Fe)/Fe_3O_4 composite such as OH and carboxylate and

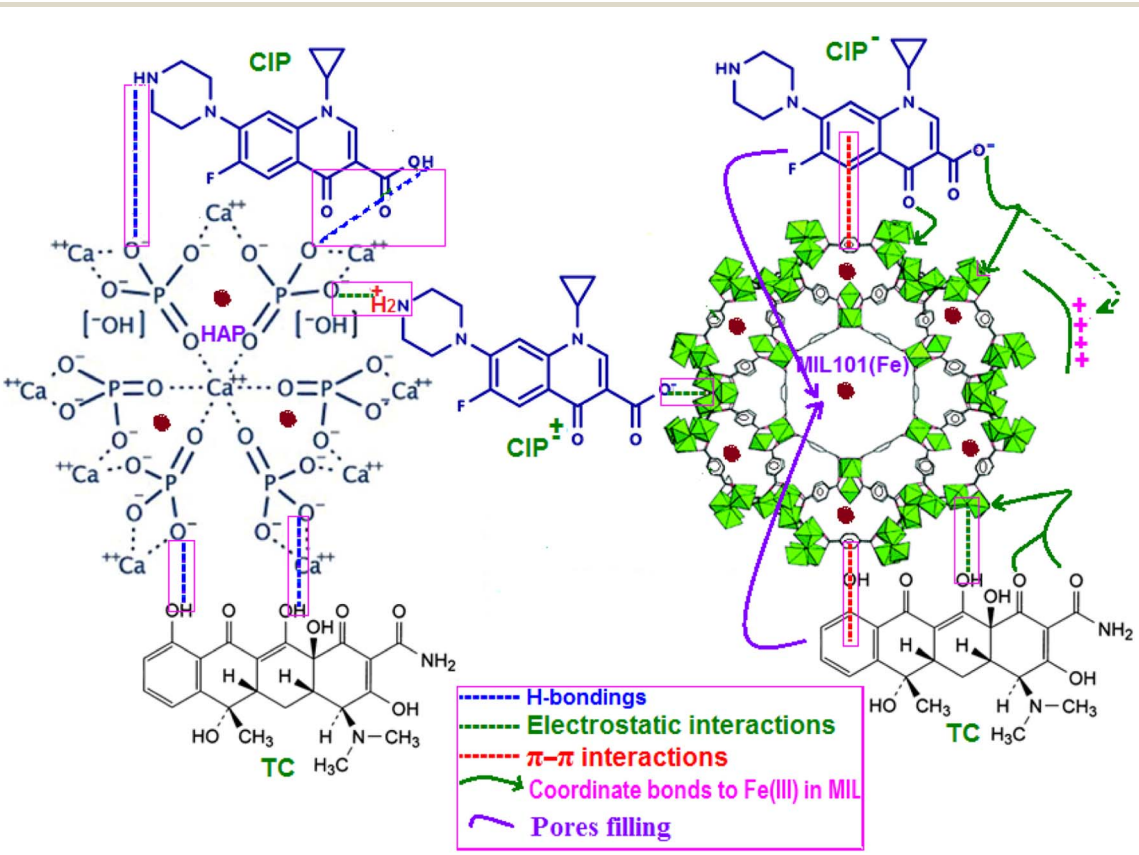

Fig. 13 Schematic diagram of the suggested adsorption mechanism of TC and CIP on HAP/MIL-101(Fe)/Fe_3O_4 nanocomposite.

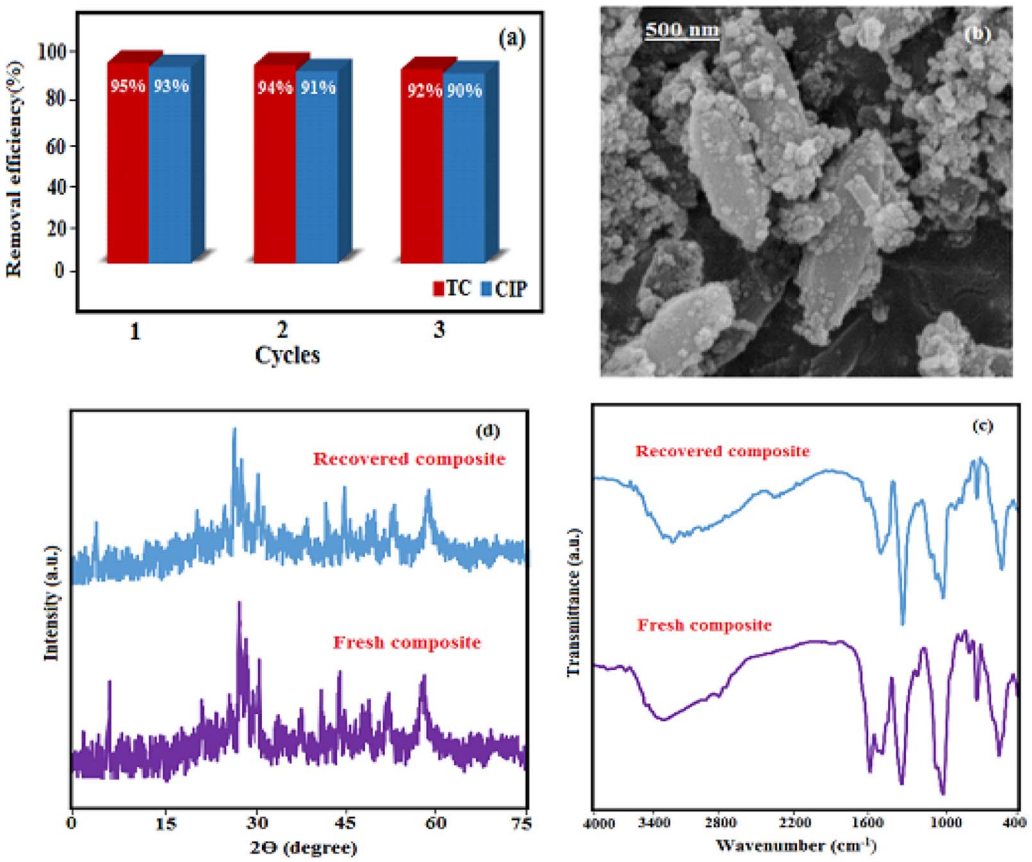

Fig. 14 (a) Reusability of the HAP/MIL-101(Fe)/Fe_3O_4 nanocomposite in the removal of TC and CIP antibiotics, (b) SEM image, (c) FT-IR spectrum and (d) XRD patterns of the fresh and recovered nanocomposite after three runs.

phosphate.[62] Therefore, electrostatic attraction, π–π interaction and hydrogen bonding play a key role in the adsorption of pollutants on HAP/MIL-101(Fe)/Fe_3O_4 as is illustrated in Fig. 13.[63,64] Evidently, a more detailed and conclusive adsorption mechanism should be further studied.

3.12. Reusability of magnetic nanocomposite

To evaluate the reusability of the HAP/MIL-101(Fe)/Fe_3O_4 nanocomposite, three cycles of antibiotic removal were performed under identical and optimized conditions. Fig. 14 shows the results of this examination. For this goal, 30 mg of nanocomposite was added into 50 mL of antibiotic solutions (50 mg L^{-1}) and was then stirred for 30 min, in continuing an external magnet was used for separating the magnetic nanocomposite from the antibiotic solution. Then, the magnetic adsorbent was washed with deionized water and ethanol several times and finally dried for 12 h at 70 °C and reused. The results in Fig. 14(a) demonstrated that the decrease in the removal efficiency was not significant for three successive cycles. Furthermore, the structural stability the recovered adsorbent was confirmed by FT-IR, XRD, and SEM after three runs as shown in Fig. 14(b)–(d). These results confirmed that the structure of the magnetic nanocomposite was stable under the reaction conditions and was not affected by the reactants.

4. Conclusions

In summary, a novel HAP/MIL-101(Fe)/Fe_3O_4 ternary nanocomposite was successfully prepared. HAP nanorods were functionalized with MIL-101(Fe) and Fe_3O_4 nanoparticles. The tests showed that the magnetic nanocomposite offers high removal efficiency against TC and CIP antibiotics. Various influential parameters on the adsorption capacity such as initial drug concentration, adsorbent dosage, temperature, and pH were evaluated. The main adsorption mechanisms were pores filling, electrostatic interaction and π–π interaction. TC and CIP adsorption processes onto the HAP/MIL-101(Fe)/Fe_3O_4 were the endothermic and spontaneous. Also, reusability tests showed that HAP/MIL-101(Fe)/Fe_3O_4 composite could be reused for three cycles without a considerable reduction in its performance. Therefore, magnetic nanocomposite can be used as an adsorbent to remove TC and CIP from water.

Conflicts of interest

There are no conflicts to declare.

Acknowledgements

The authors give their sincere thanks to the Lorestan University and Iran Nanotechnology Initiative Council (INIC) for all provided supports.

References

1 I. Lung, M. L. Soran, A. Stegarescu, O. Opris, S. Gutoiu, C. Leostean, M. D. Lazar, I. Kacso, T. D. Silipas and A. S. Porav, Evaluation of CNT-COOH/MnO_2/Fe_3O_4 nanocomposite for ibuprofen and paracetamol removal from aqueous solutions, *J. Hazard. Mater.*, 2021, **403**, 123528.

2 Z. A. Alothman, A. Y. Badjah, O. M. L. Alharbi and I. Ali, Copper carboxymethyl cellulose nanoparticles for efficient removal of tetracycline antibiotics in water, *Environ. Sci. Pollut. Res.*, 2020, **27**, 42960–42968.

3 R. Zandipak and S. Sobhanardakani, Novel mesoporous Fe_3O_4/SiO_2/CTAB–SiO_2 as an effective adsorbent for the removal of amoxicillin and tetracycline from water, *Clean Technol. Environ. Policy*, 2018, **20**, 871–885.

4 J. Li, G. Yu, L. Pan, C. Li, F. You, S. Xie, Y. Wang, J. Ma and X. Shang, Study of ciprofloxacin removal by biochar obtained from used tea leaves, *J. Environ. Sci.*, 2018, **73**, 20–30.

5 Y. Zhou, Y. He, Y. He, X. Liu, B. Xu, J. Yu, C. Dai, A. Huang, Y. Pang and L. Luo, Analyses of tetracycline adsorption on alkali-acid modified magneticbiochar: site energy distribution consideration, *Sci. Total Environ.*, 2019, **650**, 2260–2266.

6 S. Shao, Y. Hu, J. Cheng and Y. Chen, Biodegradation mechanism of tetracycline (TEC) by strain Klebsiella sp. SQY5 as revealed through products analysis and genomics, *Ecotoxicol. Environ. Saf.*, 2019, **185**, 109676.

7 C. Li, H. Lin, A. Armutlulu, R. Xie, Y. Zhang and X. Meng, Hydroxylamine-assisted catalytic degradation of ciprofloxacin in ferrate/persulfate system, *Chem. Eng. J.*, 2019, **360**, 612–620.

8 H. Yi, C. Lai, X. Huo, L. Qin, Y. Fu, S. Liu, L. Li, M. Zhang, M. Chen and G. Zeng, H_2O_2-free photo-Fenton system for antibiotics degradation in water *via* the synergism of oxygenen riched graphitic carbon nitride polymer and nano manganese ferrite, *Environ. Sci.: Nano*, 2022, **9**, 815–826; M. Shoorangiz, M. R. Nikoo, M. Salari, G. R. Rakhshandehroo and M. Sadegh, Optimized electro-fenton process with sacrificial stainless steel anode for degradation/mineralization of Ciprofloxacin, *Process Saf. Environ. Prot.*, 2019, **132**, 340–350.

9 A. Hassani, A. Khataee, M. Fathinia and S. Karaca, Photocatalytic ozonation of ciprofloxacin from aqueous solution using TiO_2/MMT nanocomposite: nonlinear modeling and optimization of the process *via* artificial neural network integrated genetic algorithm, *Process Saf. Environ. Prot.*, 2018, **116**, 365–376.

10 D. A. Palacio, L. M. Leiton, B. F. Urbano and B. L. Rivas, Tetracycline removal by polyelectrolyte copolymers in conjunction with ultrafiltration membranes through liquid-phase polymer-based retention, *Environ. Res.*, 2020, **182**, 109014.

11 J. Liu, B. Zhou, H. Zhang, J. Ma, B. Mu and W. Zhang, A novel biochar modified by chitosan-Fe/S for tetracycline adsorption and studies on site energy distribution, *Bioresour. Technol.*, 2019, **294**, 122152.

12 Y. Dai, K. Zhang, X. Meng, J. Li, X. Guan, Q. Sun, Y. Sun, W. Wang, M. Lin, M. Liu, S. Yang, Y. Chen, F. Gao, X. Zhang and Z. Liu, New use for spent coffee ground as an adsorbent for tetracycline removal in water, *Chemosphere*, 2019, **215**, 163–172.

13 M. Fang Li, Y. Guo Liu, S. Bo Liu, G. Ming Zeng, X. Jiang Hu, X. Fei Tan, L. Hua Jiang, N. Liu, J. Wen and X. Hui Liu, Performance of magnetic graphene oxide/diethylenetriaminepenta acetic acid nanocomposite for the tetracycline and ciprofloxacin adsorption in single andbinary systems, *J. Colloid Interface Sci.*, 2018, **521**, 150–159.

14 L. Chen, T. Yuan, R. Ni, Q. Yue and B. Gao, Multivariate optimization of ciprofloxacin removal by polyvinylpyrrolidon estabilized NZVI/Cu bimetallic particles, *Chem. Eng. J.*, 2019, **365**, 183–192.

15 T. Selmi, A. Sanchez-Sanchez, P. Gadonneix, J. Jagiello, M. Seffen, H. Sammouda, A. Celzard and V. Fierro, Tetracycline removal with activated carbons produced by hydrothermal carbonisation of agave americanafibres and mimosa tannin, *Ind. Crops Prod.*, 2018, **115**, 146–157.

16 V. Dutta, P. Singh, P. Shandilya, S. Sharma, P. Raizada, A. K. Saini, V. K. Gupta, A. Hosseini-Bandegharaei, S. Agarwal and A. Rahmani-Sani, Review on advances in photocatalytic water disinfection utilizing graphene and graphene derivatives-based nanocomposites, *J. Environ. Chem. Eng.*, 2019, **7**, 103132.

17 D. N. R. de Sousa, S. Insa, A. A. Mozeto, M. Petrovic, T. F. Chaves and P. S. Fadini, Equilibrium and kinetic studies of the adsorption of antibiotics from aqueous solutions onto powdered zeolites, *Chemosphere*, 2018, **205**, 137–146.

18 K. S. D. Premarathna, A. U. Rajapaksha, N. Adassoriya, B. Sarkar, N. M. S. Sirimuthu, A. Cooray, Y. S. Ok and M. Vithanage, Clay-biochar composites for sorptive removal of tetracycline antibiotic inaqueous media, *J. Environ. Manage.*, 2019, **238**, 315–322.

19 M. Beiranvand, S. Farhadi and A. Mohammadi, Graphene oxide/hydroxyapatite/silver (rGO/HAP/Ag) nanocomposite: synthesis, characterization, catalytic and antibacterial activity, *Int. J. Nano Dimens.*, 2019, **10**(2), 180–194.

20 Y. Xu, L. An, L. Chen, H. Xu, D. Zeng and G. Wang, Controlled hydrothermal synthesis of strontium-substituted hydroxyapatite nanorods and their application as a drug carrier for proteins, *Adv. Powder Technol.*, 2018, **29**, 1042–1048.

21 K. W. Jung, S. Y. Lee, J. W. Choi and Y. J. Lee, A facile one-pot hydrothermal synthesis of hydroxyapatite/biochar nanocomposites: adsorption behavior and mechanisms for the removal of copper(II) from aqueous media, *Chem. Eng. J.*, 2019, **369**, 529–541.

22 G. S. Kumar, G. Karunakaran, E. K. Girija, E. Kolesnikov, N. Van Minh, M. V. Gorshenkov and D. Kuznetsov, Size and morphology-controlled synthesis of mesoporous hydroxyapatite nanocrystals by microwave-assisted hydrothermal method, *Ceram. Int.*, 2018, **44**, 11257–11264.

23 D. G. Syarif, D. H. Prajitno, A. Kurniawan, M. B. Febrian and R. Lesmana, Hydrothermally synthesis and characterization of HAP and Zr-doped HAP nanoparticles from bovine bone and zircon for photodynamictherapy, *Process. Appl. Ceram.*, 2021, **15**, 146–153.

24 A. Jarrah and S. Farhadi, $K_6P_2W_{18}O_{62}$ encapsulated into magnetic Fe_3O_4/MIL-101(Cr) metal–organic framework: a novel magnetically recoverable nanoporous adsorbent for ultrafast treatment of aqueous organic pollutants solutions, *RSC Adv.*, 2018, **8**, 37976–37992.

25 Y. Guo, C. Feng, S. Qiao, S. Wang, T. Chen, L. Zhang, Y. Zhao and J. Wang, Magnetic Fe_3O_4-encapsulated VAN@MIL-101(Fe) with mixed-valence sites and mesoporous structuresas efficient bifunctional water splitting photocatalysts, *Nanoscale*, 2020, **12**, 12551–12560.

26 X. Ke, X. Song, N. Qin, Y. Cai and F. Ke, Rational synthesis of magnetic Fe_3O_4@MOF nanoparticles for sustained drug delivery, *J. Porous Mater.*, 2019, **26**, 813–818.

27 Q. Gong, Y. Liu and Z. Dang, Core–shell structured Fe_3O_4@GO@MIL-100(Fe) magnetic nanoparticles as heterogeneous photo-fenton catalyst for 2,4-dichlorophenol degradation under visible light, *J. Hazard. Mater.*, 2019, **371**, 677–686.

28 A. Lajevardi, M. Hossaini Sadr, M. Tavakkoli Yaraki, A. Badiei and M. Armaghan, pH-Responsive and magnetic Fe_3O_4@silica@MIL-100(Fe)/β-CD nanocomposite as drug nanocarrier: loading and release study of cephalexin, *New J. Chem.*, 2018, **42**, 9690–9701.

29 L. Pang, P. Yang, H. Yang, L. Ge, J. Xiao and Y. Zhou, Application of Fe_3O_4@MIL-100(Fe) core–shell magneticmicrospheres forevaluating the sorption of organophosphate esters to dissolved organicmatter (DOM), *Sci. Total Environ.*, 2018, **626**, 42–47.

30 B. Han, E. Zhang and G. Cheng, Facile preparation of graphene oxide-MIL-101(Fe) composite for the efficient capture of uranium, *Appl. Sci.*, 2018, **8**, 2270.

31 J. Lin, H. Hu, N. Gao, J. Ye, Y. Chen and H. Ou, Fabrication of GO@MIL-101(Fe) for enhanced visible-light photocatalysis degradation of organophosphorus contaminant, *J. Water Process Eng.*, 2020, **33**, 101010.

32 A. Jarrah and S. Farhadi, Dawson-type polyoxometalate incorporated into nanoporous MIL-101(Cr): preparation, characterization and application for ultrafast removal of organic dyes, *Acta Chim. Slov.*, 2019, **66**, 85–102.

33 D. Karthickraja, S. Karthi, G. A. Kumar, D. K. Sardar, G. C. Dannangoda, K. S. Martirosyan and E. K. Girija, Fabrication of core-shell $CoFe_2O_4$@HAP nanoparticles: a novel magnetic platform for biomedical applications, *New J. Chem.*, 2019, **43**, 13584–13593.

34 A. Jarrah and S. Farhadi, Encapsulation of $K_6P_2W_{18}O_{62}$ into magnetic nanoporous Fe_3O_4/MIL-101(Fe) for highly enhanced removal of organic dyes, *J. Solid State Chem.*, 2020, **285**, 121264.

35 S. Saire-Saire, S. Garcia-Segura, C. Luyo, L. H. Andrade and H. Alarcon, Magnetic bio-nanocomposite catalysts of $CoFe_2O_4$/hydroxyapatite-lipase for enantioselective synthesis provide aframework for enzyme recovery and reuse, *Int. J. Biol. Macromol.*, 2020, **148**, 284–291.

36 Y. Yang, F. Xia, Y. Yang, B. Gong, A. Xie, Y. Shen and M. Zhu, Litchi-like Fe_3O_4@Fe-MOF capped with HAP gatekeepers forpH-triggered drug release and anticancer effect, *J. Mater. Chem. B*, 2017, **5**, 8600–8606.

37 Y. Ma, M. Li, P. Li, L. Yang, L. Wu, F. Gao, X. Qi and Z. Zhang, Hydrothermal synthesis of magnetic sludge biochar for tetracycline and ciprofloxacin adsorptive removal, *Bioresour. Technol.*, 2021, **319**, 124199.

38 M. E. Peñafiel, E. Vanegas, D. Bermejo, J. M. Matesanz and M. P. Ormad, Organic residues as adsorbent for the removalof ciprofloxacin from aqueous solution, *Hyperfine Interact.*, 2019, **240**, 1–12.

39 K. Pakzad, H. Alinezhad and M. Nasrollahzadeh, Euphorbia polygonifoliaextract assisted biosynthesis of Fe_3O_4@CuO nanoparticles: applications in the removal of metronidazole, ciprofloxacin and cephalexin antibiotics from aqueous solutions under UV irradiation, *Appl. Organomet. Chem.*, 2020, **34**, 1–15.

40 J. Miao, F. Wang, Y. Chen, Y. Zhu, Y. Zhou and S. Zhang, The adsorption performance of tetra cyclines on magnetic graphene oxide: a novel antibiotics absorbent, *Appl. Surf. Sci.*, 2019, **475**, 549–558.

41 S. K. Sahoo, S. Padhiari, S. K. Biswal, B. B. Panda and G. Hota, Fe_3O_4 nanoparticles functionalized GO/g-C_3N_4 nanocomposite: an efficient magnetic nanoadsorbent for adsorptive removal of organic pollutants, *Mater. Chem. Phys.*, 2020, **244**, 122710.

42 M. Foroughi, M. H. Ahmadi-Azqhandi and S. Kakhki, Bio-inspired, high, and fast adsorption of tetracycline from aqueous media using Fe_3O_4-g-CN@PEI-β-CD nanocomposite: modeling byresponse surface methodology (RSM), boosted regression tree (BRT),and general regression neural network (GRNN), *J. Hazard. Mater.*, 2020, **388**, 121769.

43 W. Xiong, G. Zeng, Z. Yang, Y. Zhou, C. Zhang, M. Cheng, Y. Liu, L. Hu, J. Wan, C. Zhou, R. Xu and X. Li, Adsorption of tetracycline antibiotics from aqueous solutions on nanocomposite multi-walled carbon nanotube functionalized MIL-53(Fe) as new adsorbent, *Sci. Total Environ.*, 2018, **627**, 235–244.

44 C. Oliveira, A. L. M. de Oliveira, L. Chantelle, R. Landers, S. Medina-Carrasco, M. Del Mar Orta, E. C. Silva Filho and M. G. Fonseca, Zinc(II) modified hydroxyapatites for tetracycline removal: Zn(II) doping or ZnO deposition and their influence in the adsorption, *Polyhedron*, 2021, **194**, 114879.

45 G. Yang, Q. Gao, S. Yang, S. Yin, X. Cai, X. Yu, S. Zhang and Y. Fang, Strong adsorption of tetracycline hydrochloride on magnetic carbon-coated cobalt oxide nanoparticles, *Chemosphere*, 2020, **239**, 124831.

46 T. Ahamad, R. Ruksana, A. A. Chaudhary, M. Naushad and S. M. Alshehri, Fabrication of $MnFe_2O_4$ nanoparticles embedded chitosan-diphenylureaformaldehyderesin for the removal of tetracycline from aqueous solution, *Int. J. Biol. Macromol.*, 2019, **134**, 180–188.

47 V. T. Nguyen, T. B. Nguyen, C. W. Chen, C. M. Hung, C. P. Huang and C. Di Dong, Cobalt-impregnated biochar (Co-SCG) for heterogeneous activation of peroxymonosulfate for removal of tetracycline in water, *Bioresour. Technol.*, 2019, **292**, 121954.

48 W. A. Khanday and B. H. Hameed, Zeolite-hydroxyapatite-activated oil palm ash composite for antibiotic tetracycline adsorption, *Fuel*, 2018, **215**, 499–505.

49 J. Bao, Y. Zhu, S. Yuan, F. Wang, H. Tang, Z. Bao, H. Zhou and Y. Chen, Adsorption of tetracycline with reduced graphene oxide decorated with $MnFe_2O_4$ nanoparticles, *Nanoscale Res. Lett.*, 2018, **13**, 396.

50 A. Chandrasekaran, C. Patra, S. Narayanasamy and S. Subbiah, Adsorptive removal of ciprofloxacin and amoxicillin from single and binary aqueous systems using acid-activated carbon from prosopis juliflora, *Environ. Res.*, 2020, **188**, 109825.

51 Z. Li, M. Ma, S. Zhang, Z. Zhang, L. Zhou, J. Yun and R. Liu, Efficiently removal of ciprofloxacin from aqueous solutionby MIL-101(Cr)-HSO_3: the enhanced electrostatic interaction, *J. Porous Mater.*, 2020, **27**, 189–204.

52 A. Azizi, Green synthesis of iron oxide/cellulose magnetic recyclable nanocomposite and its evaluation in ciprofloxacin removal from aqueous solutions, *J. Iran. Chem. Soc.*, 2021, **18**, 331–341.

53 A. A. Mohammed, T. J. Al-Musawi, S. L. Kareem, M. Zarrabi and A. M. Al-Ma'abreh, Simultaneous adsorption of tetracycline, amoxicillin, and ciprofloxacin by pistachio shellpowder coated with zinc oxide nanoparticles, *Arabian J. Chem.*, 2019, **13**, 4629–4643.

54 M. K. Mohammadi-Nodeh, S. Soltani, S. Shahabuddin, H. Rashidi Nodeh and H. Sereshti, Equilibrium, kinetic and thermodynamic study of magnetic polyaniline/graphene oxide based nanocomposites for ciprofloxacin removal from water, *J. Inorg. Organomet. Polym. Mater.*, 2018, **28**, 1226–1234.

55 M. E. Mahmoud, S. R. Saad, A. M. El-Ghanam and R. H. A. Mohamed, Developed magnetic Fe_3O_4-MoO_3-AC nanocomposite for effective removal ofciprofloxacin from water, *Mater. Chem. Phys.*, 2021, **257**, 123454.

56 R. Natarajan, K. Saikia, S. K. Ponnusamy, A. K. Rathankumar, D. S. Rajendran, S. Venkataraman, D. B. Tannani, V. Arvind, T. Somanna, K. Banerjee, N. Mohideen and V. K. Vaidyanathan, Understanding the factors affecting adsorption of pharmaceuticals on different adsorbents- a critical literature update, *Chemosphere*, 2022, **287**, 131958.

57 T. Hu, Q. Jia, S. He, S. Shan, H. Su, Y. Zhi and L. He, Novel functionalized metal-organic framework MIL-101 adsorbent forcapturing oxytetracycline, *J. Alloys Compd.*, 2017, **727**, 114–122.

58 J. Yu, W. Xiong, X. Li, Z. Yang, J. Cao, M. Jia, M. R. Xu and Y. Zhang, Functionalized MIL-53(Fe) as efficient adsorbents for removal of tetracyclineantibiotics from aqueous solution, *Microporous Mesoporous Mater.*, 2019, **290**, 109642.

59 X. Liu, B. Liu, J. F. Eubank and Y. Liu, Adsorption behavior and structure transformation of mesoporous metal–organic frameworks towards arsenates and organic pollutants in aqueous solution, *Mater. Chem. Front.*, 2018, **2**, 1389–1396.

60 Y. Dong, T. Hu, M. Pudukudy, H. Su, L. Jiang, S. Shan and Q. Jia, Influence of microwave-assisted synthesis on the structural and textural properties ofmesoporous MIL-101(Fe) and NH_2-MIL-101(Fe) for enhanced tetracycline adsorption, *Mater. Chem. Phys.*, 2020, **251**, 123060.

61 N. Tian, Q. Jia, H. Su, Y. Zhi, A. Ma, J. Wu and S. Shan, The synthesis of mesostructured NH_2-MIL-101(Cr) and kineticand thermodynamic study in tetracycline aqueous solutions, *J. Porous Mater.*, 2016, **23**, 1269–1278.

62 X. Jia, S. Li, Y. Wang, T. Wang and X. Hou, Adsorption behavior and mechanism of sulfonamide antibiotics in aqueous solution on a novel MIL-101(Cr)@GO composite, *J. Chem. Eng. Data*, 2019, **64**, 1265–1274.

63 Y. Sun, M. Chen, H. Liu, Y. Zhu, D. Wang and M. Yan, Adsorptive removal of dye and antibiotic from water with functionalized zirconium-based metal organic framework and graphene oxide composite nanomaterial UiO-66-$(OH)_2$/GO, *Appl. Surf. Sci.*, 2020, **525**, 146614.

64 W. Xiong, Z. Zeng, X. Li, G. Zeng, R. Xiao, Z. Yang, Y. Zhou, C. Zhang, M. Cheng, L. Hu, C. Zhou, L. Qin, R. Xu and Y. Zhang, Multi-walled carbon nanotube/amino-functionalized MIL-53(Fe) composites: remarkable adsorptive removal of antibiotics from aqueous solutions, *Chemosphere*, 2018, **210**, 1061–1069.